ADVANCED ENERGY MATERIALS

Supporting Information

for *Adv. Energy Mater.,* DOI: 10.1002/aenm.201402307

Multiphase Nanostructure of a Quinary Metal Oxide Electrocatalyst Reveals a New Direction for OER Electrocatalyst Design

Joel A. Haber, Eitan Anzenburg, Junko Yano, Christian Kisielowski,* and John M. Gregoire**

Multi-phase nanostructure of a quinary oxide electrocatalyst reveals a new direction for OER electrocatalysis design

Joel A. Haber, Eitan Anzenburg, Junko Yano, Christian Kisielowski,* John M. Gregoire*[*]

Supplementary Information:

Table of Contents

Materials and Methods

Preparation of precursor ink solutions. Four separate metal inks, of the type previously described by Fan and Stuckey,[3,35] were prepared by mixing 5 mmoles of each of the Ni, Fe, Co, and Ce precursor with 0.80 g Pluronic F127 (Aldrich), 1.0 mL glacial acetic acid (T.J. Baker, Inc.), 0.40 mL of concentrated HNO_3 (EMD), and 30 mL of 200 proof Ethanol (Koptec). The metal precursors were $Ni(NO_3)_2$-$6H_2O$ (1.53 g, 99.999%, Sigma Aldrich), $Fe(NO_3)_3$-$9H_2O$ (2.14 g, ≥98% , Sigma Aldrich), $Co(NO_3)_2$-$6H_2O$ (1.46 g, 99.99%, Sigma Aldrich), and $Ce(NO_3)_3$-$6H_2O$ (2.22 g, 99.99%, Sigma Aldrich).

Preparation of catalyst on glassy carbon. The $Ni_{30}Fe_7Co_{20}Ce_{43}$ composition was printed onto glassy carbon rotating disk electrodes (GC RDEs, SIGRADUR G, HTW Hochtemperatur-Werkstoffe GmbH), which are cylinders 5 mm in diameter and 4 mm in height. Four separate metal inks were prepared as described above and printed at 2880 x 1440 dpi, at 7.5 nmoles of metal per mm^2. After printing, the inks were dried and the metal precursors converted to oxides by calcination in air at 40 °C for 18 h, then at 70 °C for 24 h, followed by a 5 h ramp and 10 h soak at 350 °C.

Preparation of catalyst powder. Powders were prepared by first combining the inks prepared above: 3.0 mL Ni ink, 0.7 mL Fe ink, 2.0 mL Co ink, and 4.3 mL of Ce ink. The combined ink was a stable, clear solution, which was poured into a100 mm diameter petri dish to form a think liquid film. The bulk ink solution was dried and converted to the oxide identically to the libraries and RDEs described above by heating in air at 40 °C for 18 h, then at 70 °C for 24 h, followed by a 5 h ramp and 10 h soak at 350 °C. Approximately 0.2 g of the resultant black powder was collected, with small portions used for the TEM, XAS and XRD studies reported here. Another $Ni_{30}Fe_7Co_{20}Ce_{43}$ combined ink compositions was prepared and processed at 40 °C, 70 °C, and then 450 °C, similarly to the powder above. The collected powder was used only for the XRD pattern of 450 °C powder shown in **Figure S3**.

Preparation of FeO_x and CoO_x powders from the ink precursors. Powders were prepared by placing a few mL of individual, single metal inks prepared as described above into 100 mm diameter petri dishes and processing them at 40 °C, 70 °C, and then 450 °C, similarly to the powders described above. The collected powder was analyzed by TEM, as shown in **Figure S2**.

Powder XRD collection. ~30 mg of the powders prepared above were ground in an agate mortar and pestle with MeOH and then pressed into a 0.2 mm deep by 10 mm diameter depression in a 24.6 mm diameter by 1.0 mm thick zero diffraction single crystal Si holder. (MTI corporation, SiZero24D10C1-cavity). X-ray diffraction data was collected using a Bruker D8 Discover with a IuS micro-focused source (50kV, 1mA, Cu Kalpha line with Montell mirror) and Våntec 500 2D-detector. X-ray diffraction was collected on 350 °C and 450 °C calcined $Ni_{30}Fe_7Co_{20}Ce_{43}$ powders. As seen **in Figure S3**, the powder calcined at 350 °C produces broad but clear peaks corresponding to CeO_2. The peaks corresponding to MeO are small, broad and barely discernable. The powder calcined at 450 °C produces sharper peaks corresponding to CeO_2 and one or more of the very similar (Ni-Fe-Co)O_x phases in the NaCl structure.

Electrochemical analysis of catalysts on glassy carbon rotating disk electrodes. GC RDE electrodes coated with catalyst were subjected to a series of electrochemical measurements in oxygen-saturated 1.0 M NaOH blanketed under 1 atm O_2(g). The working electrode was rotated at 1600 rpm and the counter and reference electrodes were a carbon rod (99.999%, Alfa Aesar), and a commercial saturated calomel electrode (SCE) (CH-Instruments), respectively.

All measurements were conducted in a modified two-chamber U-cell in which the first chamber held the working and reference electrodes in *ca.* 120 mL of solution, and the second chamber held the auxiliary electrode in *ca.* 25 mL. The two chambers were separated by a fine-porosity glass frit. The cell was purged for *ca.* 20 min with O_2 prior to each set of experiments. During static-voltammetry measurements, the solution in the first chamber was blanketed under O_2. During rotating-disk electrode voltammetry measurements, the solution in the first chamber was continuously bubbled with O_2. The uncompensated resistance of the cell was measured with a single-point high-frequency impedance measurement and IR drop was compensated at 85% through positive feedback using the Bio-Logic EC-Lab software. The typical electrochemical cell had R_u = *ca.* 20 Ω in 1 M NaOH. Each catalyst was investigated by a CV at 10 mV s^{-1} (forward sweep shown in Figure 2), a series of 30 second controlled-current CP steps and a series of controlled-potential CA steps. The stability of the film under catalytic conditions was determined using controlled-current electrolysis. The catalyst material was held at a constant current density of 10 mA cm^{-2} for 2 h and the potential was measured as a function of time, as reported previously.

XAS Methods and Analyses. The XAS measurements at Ce L_{III}, Ni, Co, and Fe K-edges were performed on beamline 7-3 at Stanford Synchrotron Radiation Laboratory (SSRL) and on beamline 10.3.2 at Advanced Light Source (ALS). At SSRL beamline 7-3, a Si (220) double crystal was used to monochromatize the radiation and then detune the radiation to 50% of flux maximum at the edge energy, thereby attenuating the effects of higher harmonics. Fluctuations in the incident beam intensity were monitored using a N_2-filled chamber (I_0) in front of the sample. XAS spectra were also collected for the reference samples mentioned for XES and energy was calibrated using the metal foils placed between two N_2-filled chambers (I_1 and I_2) after the sample. The data was collected at room temperature in fluorescence excitation mode using a 30 element Ge detector (Canberra). At ALS beamline 10.3.2, the radiation was monochromatized by a Si (111) double-crystal monochromator. The intensity of the incident X-ray was monitored by an N_2-filled ionization chamber (I_0) in front of the sample. The energy was calculated using a glitch in I_0 relative to the absorption edge of metal foils. All data were collected at room temperature. Spectra were calibrated with respect to the first peak maximum of first derivative for metal foils of nickel (8333.0 eV), cerium (5723.0 eV), cobalt (7709.0 eV), and iron (7112.0 eV).

Data analysis was done using the standard programs based on IFEFFIT.[24] The spectra were normalized with respect to the edge height after subtracting the pre-edge and post-edge backgrounds using Athena software. To extract EXAFS oscillations, background was removed in k-space using a five-domain cubic spline. The resulting k-space data, $k^3\chi(k)$, was then Fourier transformed. EXAFS curve fitting was performed with Artemis and IFEFFIT software using *ab initio*-calculated phases and amplitudes from the program FEFF 8.2. These *ab initio* phases and amplitudes were used in the EXAFS equation:

$$\chi(k) = S_0^2 \sum_j \frac{N_j}{kR_j^2} f_{eff_j}(\pi,k,R_j) e^{-2\sigma_j^2 k^2} e^{-2R_j/\lambda_j(k)} \sin(2kR_j + \phi_{ij}(k)) \qquad (1)$$

The neighboring atoms to the central atom(s) are divided into *j* shells, with all atoms with the same atomic number and distance from the central atom grouped into a single shell. Within each shell, the coordination number N_j denotes the number of neighboring atoms in shell *j* at a distance of R_j from the central atom. The term $f_{effj}(\pi,k,R_j)$ is the *ab initio* amplitude function for

shell *j*, and the Debye-Waller term $e^{-2\sigma_j^2 k^2}$ accounts for damping due to static and thermal disorder in absorber-backscatterer distances. The mean free path term $e^{-2R_j/\lambda_j(k)}$ reflects losses due to inelastic scattering, where $\lambda_j(k)$ is the electron mean free path. The oscillations in the EXAFS spectrum are reflected in the sinusoidal term, $\sin(2kR_j + \varphi_{ij}(k))$ where $\varphi_{ij}(k)$ is the *ab initio* phase function for shell *j*. S_0^2 is an amplitude reduction factor due to shake-up/shake-off processes at the central atom(s). The EXAFS equation was used to fit the experimental data using *N*, *R*, and the EXAFS Debye-Waller factor (σ^2) as variable parameters. S_0^2 was fixed to 1.0 for Ce, 0.83 for Ni, 0.75 for Co, and 0.70 for Fe. E_0 was defined as 5730 eV for Ce L_{III}, 8340 eV for Ni, 7720 eV for Co, and 7120 for Fe for the energy (eV) to wave vector (*k*, $Å^{-1}$) axis conversion.Fitting parameters for bulk standard materials (CeO_2 and NiO) and the four cations from the alloy catalyst are provided in Table S3.

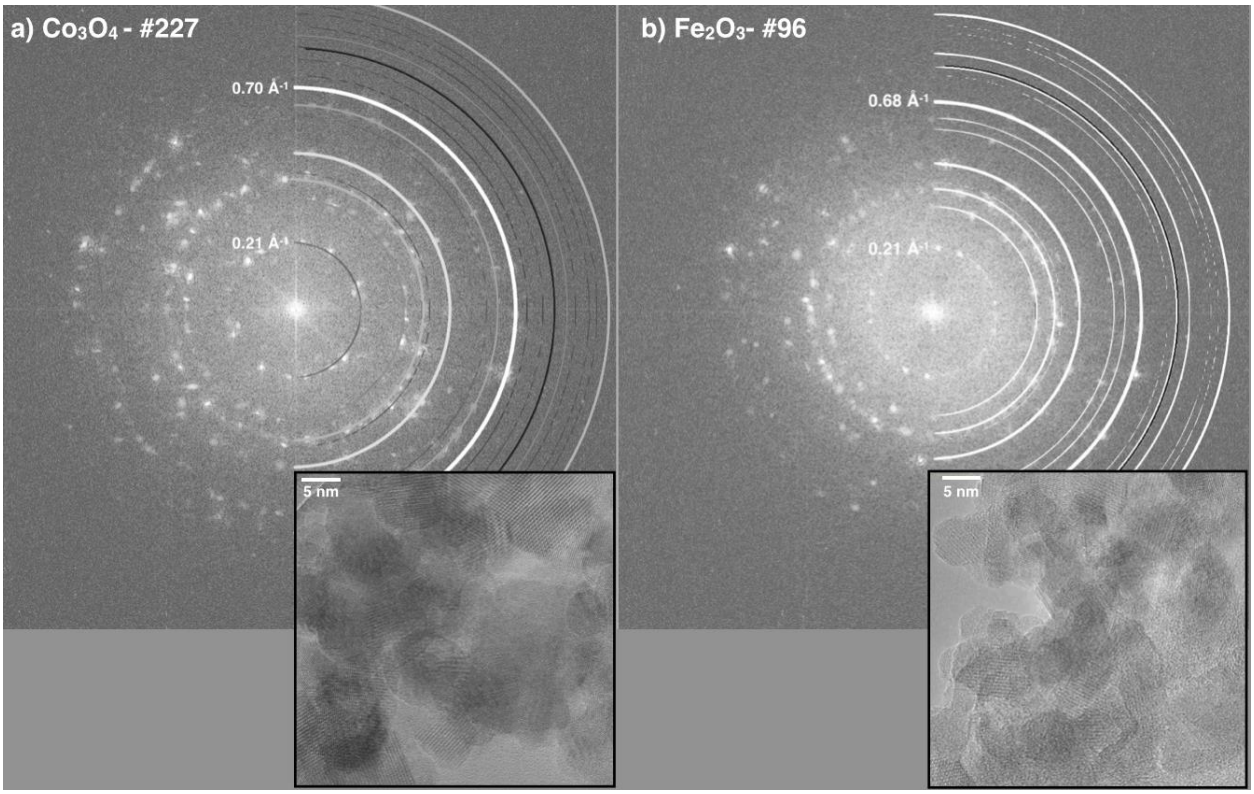

Figure S1. Fourier Transforms of individual images from Co_3O_4 (a) and Fe_2O_3 (b) recorded at Scherzer focus with 300 kV. The individual images are shown as insets and calculated ring patterns of space groups #227 and #97 are overlaid (bold lines: dominant reflections, faint lines: minor reflections).

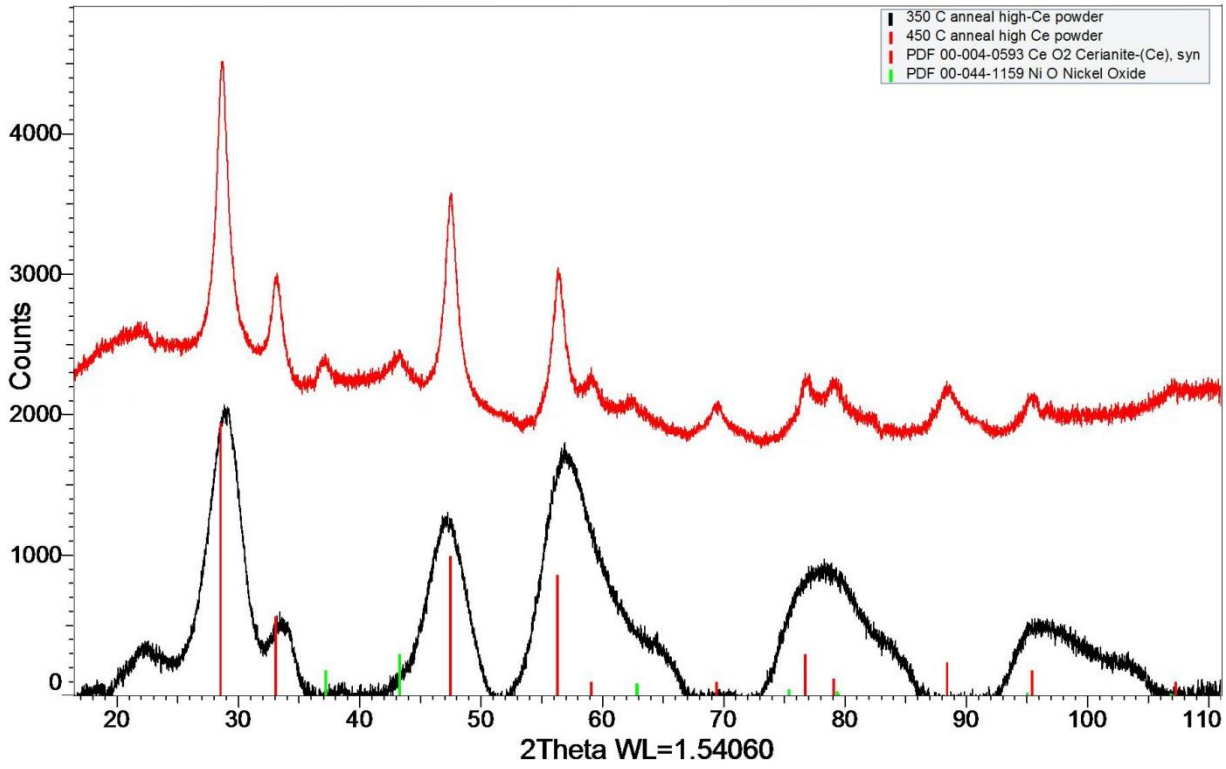

Figure S2: XRD powder patterns of $Ni_{0.3}Fe_{0.07}Co_{0.2}Ce_{0.43}O_x$ catalyst powder calcined at 350 °C (black trace at bottom) and 450 °C (red trace at top), showing the presence of CeO_2 (PDF 00-004-0593, red sticks) and NiO (PDF 00-04401159, green sticks).

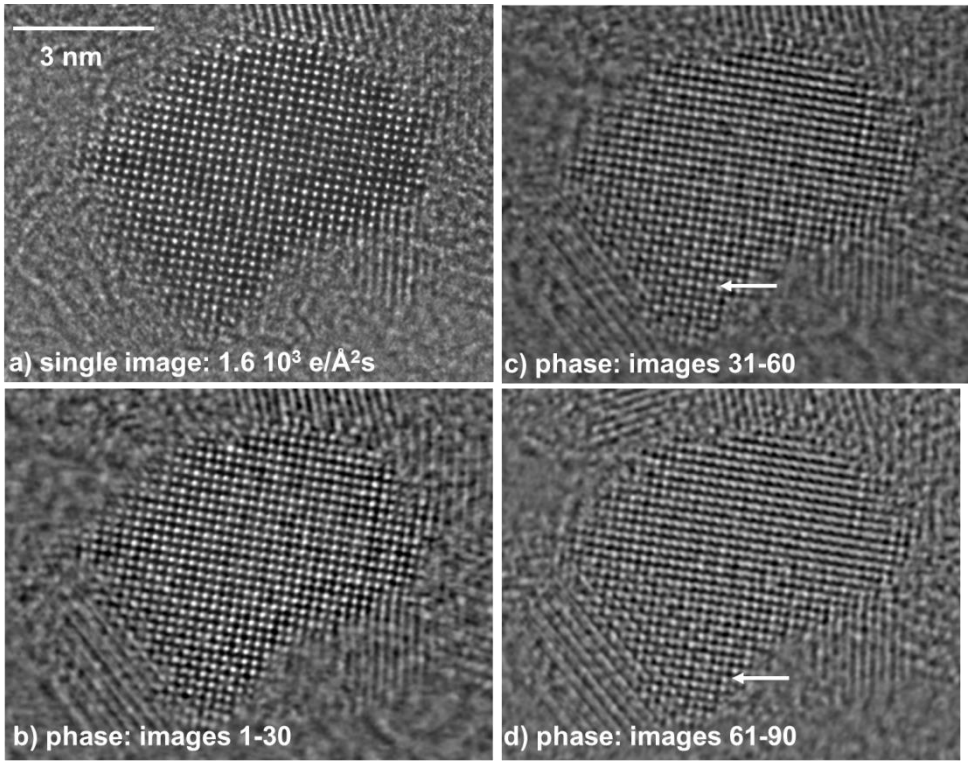

Figure S3. Contrast modifications by beam-sample interactions. a) First image from a focus series of 90 images of an uncommonly large, 5-7 nm particle recorded with a medium dose rate. b) Reconstructed phase image from the first subset of 30 images showing the same structure with an enhanced signal-to noise ratio. A direct attachment of adjacent grains becomes obvious. c), d) Reconstructed phase images from the second and third subset of 30 images, respectively. Contrast alterations (arrows) are apparent, suggesting beam-induced vacancy formation.

Table S1. A comparison of calculated and measured diffraction spots from Figure 2 b). Crystal structure data are from references [S1] and [S2].

NiO g-measured / Å^{-1}	**NiO - 225 a = 4.14 Å calculated**	**CeO_2 g-measured / Å^{-1}**	**CeO_2 - 225 a = 5.4 Å calculated**	**plane**
0.43 ± 0.01	0.42	0.31 ± 0.01	0.32	111
0.49	0.48	0.36	0.37	200
0.68	0.68	0.53	0.52	220
0.80	0.80	0.63	0.62	113
0.84	0.83	0.63	0.64	222
0.96	0.96	—	—	400

Table S2. Comparison the crystal structures of CeO_2 with the structure the transition metal oxides (MeO). The similar lattice parameters of the transition metal oxides suggests the formation of miscible alloys with all metal ions octahedrally coordinated by oxygen ions (model). CeO_2 is tetrahedrally coordinated (model) and exhibits a largely increased bond length. Crystal structure data are from references [S1, S2 and S3].

Elements	Space Group	Lattice parameter / nm	O-Me Bond length / nm
FeO	225	0.433	0.216
CoO	225	0.424	0.209
NiO	225	0.418	0.208
CeO_2	225	0.540	0.234

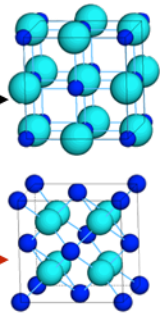

Table S3. EXAFS curve fitting parameters. N is the coordination number and σ^2 is the Debye-Waller factor. ΔE is the EXAFS threshold energy. R factor (%) indicates the goodness of the fit. Bold letters are the fixed parameters. M (in Co-M and Fe-M) assumes 2nd sphere metals. The values in parentheses indicate the uncertainty in the value.

Sample		Path	R (pm)		N	σ^2 (Å^2)	R (%)
			XRD	EXAFS			
Ce	bulk CeO_2	Ce-O	234	233 (3)	**8**	0.009 (0.002)	8.0
		Ce-Ce	383	385 (2)	**12**	0.005 (0.001)	
	$NiFeCoCeO_x$	Ce-O		229 (7)	**8**	0.020 (0.004)	13.0
		Ce-Ce		383 (7)	**12**	0.020 (0.006)	
Ni	bulk NiO	Ni-O	208	207 (2)	**6**	0.005 (0.003)	1.5
		Ni-Ni	295	2.96 (1)	**12**	0.005 (0.001)	
	$NiFeCoCeO_x$	Ni-O		205 (3)	**6**	0.009 (0.003)	7.0
		Ni-Ni		296 (3)	**12**	0.013 (0.002)	
Co	$NiFeCoCeO_x$	Co-O		191 (2)	**6**	0.006 (0.001)	5.2
		Co-M		288 (2)	**6**	0.014 (0.002)	
Fe	$NiFeCoCeO_x$	Fe-O		195 (1)	**6**	0.007 (0.001)	0.6
		Fe-M		300 (3)	**6**	0.025 (0.004)	

References

[S1] O.T. Sorensen, J. Solid State Chem. **1976**, 18, 217-233.

[S2] D. Taylor, Trans. J. Br. Ceram. Soc. **1984**, 83, 5-9.

[S3] A.T. Gordon, G. Bitsianes, T.L. Joseph *Trans. Metal. Soc. AIME* **1965**, *233*, 1519.